



Cite this: *Nanoscale*, 2020, **12**, 7509

Received 16th January 2020,  
Accepted 13th March 2020

DOI: 10.1039/d0nr00444h

rsc.li/nanoscale

## *In situ* construction of a self-assembled AIE probe for tumor hypoxia imaging†

Tianhao Xue, Kuanchun Shao, Jingyuan Xiang, Xinyi Pan, Zixuan Zhu and Yaning He \*

This communication reported a hypoxia-responsive fluorescent probe based on the *in situ* concept, which combines a water-soluble azobenzene containing copolymer with a carbamate linkage and an anionic water-soluble aggregation-induced emission fluorogen (AIEgen) tetraphenylethene (TPE). The water-soluble copolymer can be transformed into a protonated primary amine containing polymer by the reduction of the azo bond and through a 1,6-self elimination cascade reaction under hypoxic conditions. The transition of anionic TPE from the molecular dispersed state to the aggregation state induced by self-assembly with the cationic polymer would lead to an obvious increase in fluorescence according to the AIE characteristics.

In recent years, fluorescence imaging has attracted scientific interest and has been extensively investigated for potential applications in the detection of cancer, due to its superior resolution and sensitivity for the imaging of small tumor nodules.<sup>1–3</sup> Excellent selective fluorescent probes should be designed according to the characteristic traits of tumors. A variety of stimuli-responsive fluorescent probes used for tumor imaging have been explored, such as pH, redox and enzyme.<sup>4–6</sup> Most of these probes are small fluorescent molecules. Although they have the characteristics of small size and relatively good membrane permeability, the solubility and biocompatibility *in vivo* are still the tough issues under normal circumstances.<sup>7,8</sup> Despite exploring some biocompatible nano-sized fluorescent probes to overcome the disadvantages of small molecular fluorescent probes which may also accumulate at the tumor sites due to the enhanced permeability and retention (EPR) effect and the long retention time at tumor sites, they are unlikely to penetrate deeply into the solid tumor due to the difficulty in controlling the size of nanoparticles.<sup>9–12</sup> To solve this dilemma, a desirable strategy of *in situ* self-

assembly has been proposed in recent years. As per this concept, water-soluble small molecules can penetrate into tumor tissues and self-assemble into nanoparticles due to the structural change induced by a tumor microenvironment at the tumor sites, and may possess the advantage of both better permeability and a longer retention time at tumor sites.<sup>13–15</sup> To date, a number of fluorescent probes with various responsiveness according to the characteristics of the tumor sites have been explored by taking advantage of the *in situ* self-assembly concept.<sup>16–20</sup> For instance, Xu and co-workers explored a fluorescent probe of D-peptide derivatives, which can self-assemble into fluorescent nanofibrils for alkaline phosphatase (ALP) detection by the action of phosphatases at tumor sites.<sup>21</sup> Wang *et al.* designed a probe of cyanine containing peptide-based molecule, which can be activated by fibroblast activation protein- $\alpha$  to form fluorescence-enhanced nanofibers on the surface of a cancer associated fibroblast.<sup>22</sup> Ye *et al.* prepared a fluorescence and magnetic resonance bimodal probe with a phosphate group modified merocyanine, paramagnetic DOTA-Gd chelate and hydrophobic dipeptide Phe–Phe linker, which can be activated by ALP to self-assemble *in situ* at tumor sites.<sup>23</sup>

Hypoxia is one of the most important features of the tumor. As the tumor grows in an exaggerated way, the interior cells of the tumor will rapidly outgrow their blood supply, leading to a much lower oxygen concentration in the intratumor microenvironment than in healthy tissues.<sup>24–26</sup> However, to the best of our knowledge, hypoxia responsive fluorescent probes based on the *in situ* self-assembly concept have not been reported. The azobenzene moiety can be reduced efficiently by azoreductase overexpressed in a hypoxic microenvironment, and has been used as a marker for the construction of hypoxia responsive fluorescent probes for tumor hypoxia detection.<sup>27–31</sup> Furthermore, the reduction reaction of azobenzene can induce an efficient self-elimination reaction of carbamate linkage, which contributes to the formation of a protonated primary amine.<sup>32</sup> Inspired by the above reactions, we considered using the negatively charged fluorescent molecules that can self-

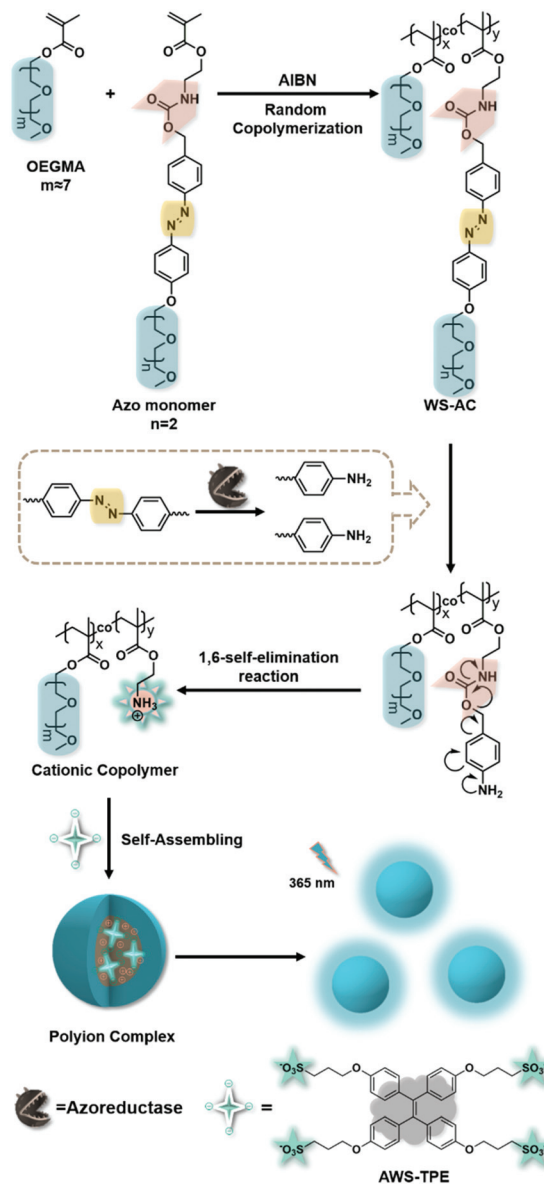
Key Laboratory of Advanced Materials (MOE), Department of Chemical Engineering, Tsinghua University, Beijing, 10084, China. E-mail: heyanying@mail.tsinghua.edu.cn

† Electronic supplementary information (ESI) available. See DOI: 10.1039/d0nr00444h

assemble *in situ* with such azo polymers by the action of azoreductase under hypoxic conditions to generate fluorescence and form nanoaggregates at tumor sites for hypoxia detection. Conventional fluorescent molecules show strong fluorescence in solution while their aggregation will decrease fluorescence or even cause quenching (ACQ) of fluorescence,<sup>33</sup> and so they cannot be used in our system. In contrast to the ACQ phenomenon, aggregation-induced emission fluorogens can show strong fluorescence in the aggregation state due to the restriction of intramolecular motions, but exhibit unobvious fluorescence in the molecular dispersed state.<sup>34–36</sup> Therefore, the negatively charged water-soluble AIEgens have the potential for *in situ* self-assembling into nanoparticles for tumor hypoxia imaging when used with the carbamate linkage modified azo polymer in a hypoxic microenvironment, which may achieve the “turn on” function of the probe.

In this communication, we explored a hypoxia-responsive probe of a water-soluble azobenzene containing copolymer (WS-AC) combined with a carbamate linkage and sulfonic acid group modified anionic water-soluble tetraphenylethene (AWS-TPE), which can be used for *in situ* tumor hypoxia imaging. Both WS-AC and AWS-TPE have good solubility in an aqueous solution. As AWS-TPE was in the molecular dispersed state in water, it could not show fluorescence due to the AIE characteristics. When the azobenzene moiety was cleaved by the azoreductase overexpressed in a hypoxic microenvironment, the 1,6-self-elimination cascade reaction occurred, contributing to the transition of the precursor polymer WS-AC from a chemically neutral state to a cationic state. Then the positively charged polymer chain which is the reduction product could form assemblies with the negatively charged AWS-TPE *in situ* owing to the electrostatic interaction. The aggregation of AWS-TPE resulted in an apparent increase of fluorescence.

Inspired by the hypoxia responsive properties of the previously studied azo copolymer,<sup>32,37</sup> we synthesized a carbamate linkage containing an azobenzene methacrylate monomer (azo monomer) with good water solubility. The precursor polymer WS-AC with excellent water solubility was synthesized *via* copolymerization of the azo monomer and the hydrophilic monomer poly(ethylene glycol) methyl ether methacrylate (OEGMA), which is shown in Scheme 1. Subsequently, AWS-TPE was obtained *via* the McMurry cross-coupling reaction of 4,4'-dihydroxybenzophenone followed by sulfonic acid group modification. The synthesis details of WS-AC and AWS-TPE are shown in the ESI (Fig. S1†). The <sup>1</sup>H NMR spectra of the azo monomer, WS-AC and AWS-TPE are shown in Fig. S2.† The characteristic peaks of WS-AC in DMSO-d<sub>6</sub> (and D<sub>2</sub>O) corresponding to the protons of the azobenzene moiety (7.04–7.90 ppm in DMSO-d<sub>6</sub> and 6.66–7.98 ppm in D<sub>2</sub>O) and oligoethylene glycol moiety (3.30–3.70 ppm in DMSO-d<sub>6</sub> and 3.33–3.87 ppm in D<sub>2</sub>O) indicate the successful construction of the hydrophilic polymer WS-AC. According to the integral area, it can be found that the ratio of the azo monomer to OEGMA is about 1 : 7. In addition, the characteristic peaks of AWS-TPE in DMSO-d<sub>6</sub> indicate that the successful construction of this



**Scheme 1** Fabrication of activatable polymeric AIE aggregates *via* self-assembly in an aqueous solution.

sulfonic acid group modified TPE as well. The number-average molecular weight of the polymer WS-AC estimated from the result of the polystyrene sample is 28 000 with a polydispersity index of 1.3. Fig. S3† reveals the UV–visible absorption spectrum of WS-AC. The AIE properties of AWS-TPE were characterized by using a fluorescence spectrophotometer in H<sub>2</sub>O/acetone mixtures with different acetone fractions (Fig. S4†). Overall, these results proved the successful construction of WS-AC and AWS-TPE.

According to the previous research, the azo bond (–N=N–) can be cleaved efficiently by azoreductase overexpressed in a hypoxic tumor microenvironment.<sup>27–31,38</sup> Enzyme treatment (NQO 1, rat liver microsomes) and chemical reagent treatment (sodium dithionite, hydrazine) are proved to be efficient ways

for the reduction of the  $-N=N-$  bond.<sup>39,40</sup> To confirm the hypoxia responsive properties of WS-AC, the UV-visible spectra of WS-AC were recorded before and after the treatment of rat liver microsomes with  $\beta$ -nicotinamide adenine dinucleotide phosphate reduced tetra(cyclohexylammonium) salt (NADPH) as the coenzyme in phosphate buffer (PBS) under hypoxic conditions. As shown in Fig. 1, the typical absorption of azobenzene at around 365 nm disappeared after the reduction reaction, confirming the destruction of the azobenzene moiety. An obvious color change from yellow to colorless could be observed with the naked eye, and is shown in the inset of Fig. 1. Then, the cleavage of the  $-N=N-$  bond induced an efficient self-elimination of carbamate linkage, which led to the formation of a stable protonated primary amine. The  $^1\text{H}$  NMR spectrum was used to confirm the product after the reduction reaction. As shown in Fig. S5,<sup>†</sup> the characteristic peaks corresponding to the protons of the azobenzene moiety disappeared after the reduction reaction, indicating the destruction of the azobenzene moiety. Besides, a typical broad signal at around 7.85 ppm was attributed to the ammonium groups, confirming the coincidence of the elimination process of carbamate linkage and the transition of WS-AC from a chemically neutral state to a cationic state. These results proved the hypoxia responsiveness of the hydrophilic copolymer and the potential of the copolymer WS-AC for assembling *in situ* with sulfonic acid modified AWS-TPE through electrostatic interaction in an aqueous system.

To further confirm whether this concept can be used for hypoxia responsive *in situ* fluorescence imaging, the fluorescence spectra of WS-AC and AWS-TPE in PBS were recorded before and after enzymatic treatment with NADPH under hypoxic conditions. As shown in Fig. 2, the fluorescence spectrum of the mixed solution of WS-AC and AWS-TPE showed no obvious emission under 365 nm excitation before the reduction reaction, indicating that AWS-TPE was in the mole-

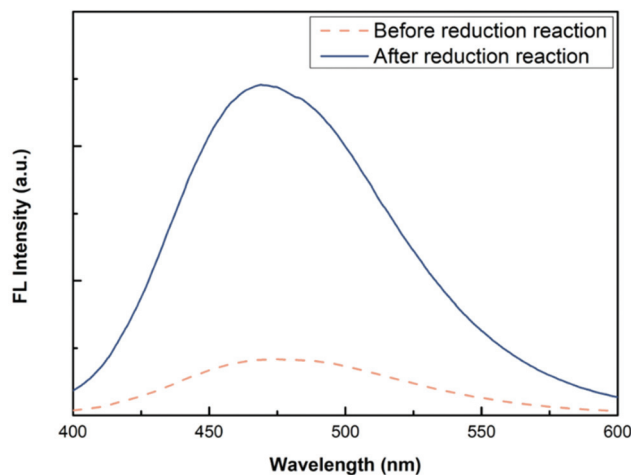


Fig. 2 Fluorescence spectra of WS-AC ( $0.1 \text{ mg mL}^{-1}$ ) and AWS-TPE ( $0.05 \text{ mg mL}^{-1}$ ) in a PBS solution before and after the enzymatic reduction reaction under hypoxic conditions.

cular dispersed state due to its good water solubility. An obvious increase in fluorescence at around 473 nm could be observed after the reduction reaction, confirming the reduction of the azobenzene moiety. This result proved that WS-AC/AWS-TPE has the potential for *in situ* tumor hypoxia imaging.

The obtained polymer WS-AC was completely soluble in an aqueous system and cannot form obvious aggregates according to the dynamic light scattering (DLS) measurement (orange dash line in Fig. S6<sup>†</sup>). To confirm the *in situ* self-assembling process, TEM imaging and DLS measurement were carried out to find whether there existed newly-formed nanoaggregates after the reduction reaction. The TEM image of the self-assembled nanoaggregates after the reduction reaction is shown in Fig. 3. Uniform nanoaggregates with a mean diameter of around 50 nm were observed (estimated statistically from the TEM image), which is consistent with the DLS measurement result (blue solid line in Fig. S6<sup>†</sup>).

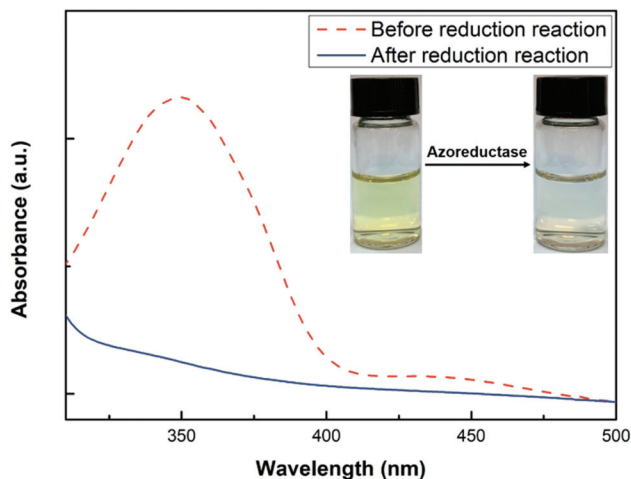


Fig. 1 UV-visible absorption spectra of the polymer WS-AC ( $0.1 \text{ mg mL}^{-1}$ ) in an aqueous solution before and after the enzymatic reduction reaction.

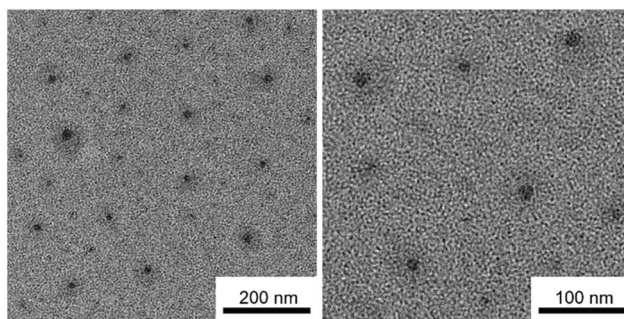
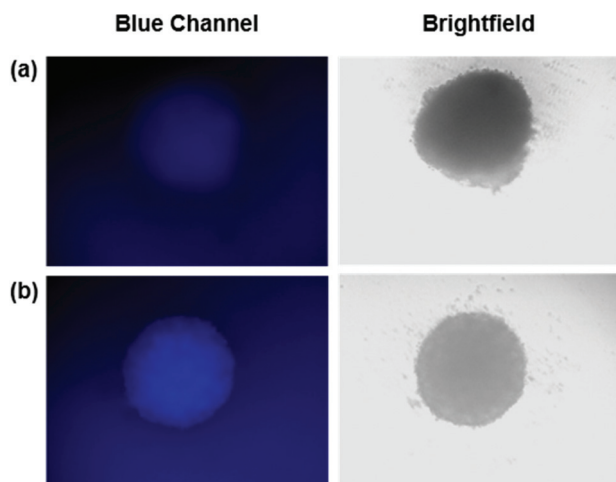


Fig. 3 Typical TEM image of the self-assembled nanoparticles with the reduction product of WS-AC ( $0.1 \text{ mg mL}^{-1}$ ) and AWS-TPE ( $0.05 \text{ mg mL}^{-1}$ ) in an aqueous solution after the reduction reaction.



**Fig. 4** Fluorescence microscopy images of HeLa multicellular tumor spheroids (MCTS) incubated with AWS-TPE only and with WS-AC/AWS-TPE after 72 h under hypoxic conditions.

All of the above results indicate that WS-AC can be reduced to a hydrophilic cationic polymer by enzyme treatment *via* the cleavage of the  $-N=N-$  bond and the subsequent 1,6-self-elimination process of carbamate linkage. This structural transition from a chemically neutral state to a cationic state can activate the fluorescence of molecularly-dispersed AWS-TPE through an electrostatic attraction induced aggregation process under hypoxic conditions to form polyion complexes *in situ*. Meanwhile, the results demonstrate that WS-AC and AWS-TPE could be used as “turn-on” *in situ* fluorescent probes triggered by azoreductase under hypoxic conditions as well.

It has been reported that azoreductase was overexpressed at hypoxic tumor sites.<sup>41,42</sup> To further investigate whether WS-AC and AWS-TPE can be used for *in situ* fluorescence imaging, we used the multicellular tumor spheroid (MCTS) model to mimic *in vivo* tumor growth.<sup>43,44</sup> The MCTSs of HeLa cells were incubated with a mixture of AWS-TPE only and with WS-AC/AWS-TPE respectively for 72 h under hypoxic conditions to confirm whether this concept can be used for *in situ* tumor hypoxia imaging *in vitro*. The fluorescence microscopy images of HeLa MCTS treated with AWS-TPE only (Fig. 4(a)) and with WS-AC/AWS-TPE (Fig. 4(b)) are shown in Fig. 4. It can be observed from Fig. 4(a) that the MCTS incubated with AWS-TPE only shows very weak fluorescence, indicating that AWS-TPE was in the molecular dispersed state, whereas the HeLa MCTS treated with WS-AC/AWS-TPE (Fig. 4(b)) shows obviously much higher fluorescence emission than the HeLa MCTS treated with AWS-TPE only, indicating the aggregation of anionic AWS-TPE with the cationic reduction product of WS-AC. Moreover, the intensity of fluorescence from the MCTS incubated with WS-AC/AWS-TPE was significantly enhanced after 24 hours and gradually increased with the prolonged incubation time up to 96 hours (Fig. S7†). These results proved that WS-AC/AWS-TPE can be used as a fluorescent probe for *in situ* tumor hypoxia detection.

## Conclusions

In summary, we have reported a novel strategy for the construction of an azobenzene based hypoxia-responsive fluorescent probe of the WS-AC/AWS-TPE complex for *in situ* tumor hypoxia imaging. Both WS-AC and AWS-TPE have excellent solubility in water. The *in situ* self-assembling process can be triggered by the reduction of the azobenzene moiety by the action of azoreductase overexpressed in a hypoxic microenvironment. The reduction of the azobenzene moiety can lead to the self-elimination process of carbamate linkage, which contributes to the structural transition of WS-AC from a chemically neutral state to a cationic state. Thus, the transition of AWS-TPE from the molecular dispersed state to the aggregation state was induced by self-assembly with a protonated primary amine containing polymer, which would lead to an obvious fluorescence increase. This *in situ* self-assembly process to construct the fluorescent probe has also been proved by *in vitro* experiment.

## Conflicts of interest

The authors declare that they have no conflicts of interest.

## Acknowledgements

The authors gratefully acknowledge the financial support from the National Key Research and Development Program of China (Grant No. 2017YFA0701303) and the National Natural Science Foundation of China (Grant No. 51873097 and 21674058). The authors especially thank Dr Juanjuan Du and colleagues in the School of Pharmaceutical Sciences at Tsinghua University for performing the related cell experiment and for helpful discussion.

## References

- 1 D. J. Stephens and V. J. Allan, *Science*, 2003, **300**, 82–86.
- 2 W. R. Zipfel, R. M. Williams and W. W. Webb, *Nat. Biotechnol.*, 2003, **21**, 1369–1377.
- 3 B. Ballou, L. A. Ernst and A. S. Waggoner, *Curr. Med. Chem.*, 2005, **12**, 795–805.
- 4 H. Shi, Y. Lei, J. Ge, X. He, W. Cui, X. Ye, J. Liu and K. Wang, *Anal. Chem.*, 2019, **91**, 9154–9160.
- 5 Z. Liu, X. Zhou, Y. Miao, Y. Hu, N. Kwon, X. Wu and J. Yoon, *Angew. Chem., Int. Ed.*, 2017, **56**, 5812–5816.
- 6 U. Markel, K. D. Essani, V. Besirlioglu, J. Schiffels, W. R. Streit and U. Schwaneberg, *Chem. Soc. Rev.*, 2020, **49**, 233–262.
- 7 M. Vendrell, D. Zhai, J. C. Er and Y.-T. Chang, *Chem. Rev.*, 2012, **112**, 4391–4420.
- 8 X. Qiu, L. Xu, Y. Zhang, A. Yuan, K. Wang, X. Zhao, J. Wu, H. Guo and Y. Hu, *Mol. Pharm.*, 2016, **13**, 829–838.
- 9 Z. Hai and G. Liang, *Adv. Biosyst.*, 2018, **2**, 1800108.

- 10 H. Lee, H. Fonge, B. Hoang, R. M. Reilly and C. Allen, *Mol. Pharm.*, 2010, **7**, 1195–1208.
- 11 S. D. Perrault, C. Walkey, T. Jennings, H. C. Fischer and W. C. Chan, *Nano Lett.*, 2009, **9**, 1909–1915.
- 12 H. Cabral, Y. Matsumoto, K. Mizuno, Q. Chen, M. Murakami, M. Kimura, Y. Terada, M. R. Kano, K. Miyazono, M. Uesaka, N. Nishiyama and K. Kataoka, *Nat. Nanotechnol.*, 2011, **6**, 815–823.
- 13 Z. Yang, H. Gu, D. Fu, P. Gao, J. K. Lam and B. Xu, *Adv. Mater.*, 2004, **16**, 1440–1444.
- 14 C. Ren, J. Zhang, M. Chen and Z. Yang, *Chem. Soc. Rev.*, 2014, **43**, 7257–7266.
- 15 L.-L. Li, S.-L. Qiao, W.-J. Liu, Y. Ma, D. Wan, J. Pan and H. Wang, *Nat. Commun.*, 2017, **8**, 1276.
- 16 D. Ye, A. J. Shuhendler, L. Cui, L. Tong, S. S. Tee, G. Tikhomirov, D. W. Felsher and J. Rao, *Nat. Chem.*, 2014, **6**, 519–526.
- 17 X. Liu and G. Liang, *Chem. Commun.*, 2017, **53**, 1037–1040.
- 18 H. Wang, Z. Feng, S. J. Del Signore, A. A. Rodal and B. Xu, *J. Am. Chem. Soc.*, 2018, **140**, 3505–3509.
- 19 Y.-X. Lin, S.-L. Qiao, Y. Wang, R.-X. Zhang, H.-W. An, Y. Ma, R. P. Y. J. Rajapaksha, Z.-Y. Qiao, L. Wang and H. Wang, *ACS Nano*, 2017, **11**, 1826–1839.
- 20 Z. Hai, J. Wu, D. Saimi, Y. Ni, R. Zhou and G. Liang, *Anal. Chem.*, 2018, **90**, 1520–1524.
- 21 J. Zhou, X. Du, C. Berciu, H. He, J. Shi, D. Nicastro and B. Xu, *Chem*, 2016, **1**, 246–263.
- 22 X.-X. Zhao, L.-L. Li, Y. Zhao, H.-W. An, Q. Cai, J.-Y. Lang, X.-X. Han, B. Peng, Y. Fei, H. Liu, H. Qin, G. Nie and H. Wang, *Angew. Chem.*, 2019, **131**, 15431–15438.
- 23 R. Yan, Y. Hu, F. Liu, S. Wei, D. Fang, A. J. Shuhendler, H. Liu, H.-Y. Chen and D. Ye, *J. Am. Chem. Soc.*, 2019, **141**, 10331–10341.
- 24 H. K. Eltzschig and P. Carmeliet, *N. Engl. J. Med.*, 2011, **364**, 656–665.
- 25 M. Höckel, K. Schlenger, B. Aral, M. Mitze, U. Schäffer and P. Vaupel, *Cancer Res.*, 1996, **56**, 4509–4515.
- 26 D. M. Gilkes, G. L. Semenza and D. Wirtz, *Nat. Rev. Cancer*, 2014, **14**, 430–439.
- 27 K. Kiyose, K. Hanaoka, D. Oushiki, T. Nakamura, M. Kajimura, M. Suematsu, H. Nishimatsu, T. Yamane, T. Terai, Y. Hirata and T. Nagano, *J. Am. Chem. Soc.*, 2010, **132**, 15846–15848.
- 28 W. Piao, S. Tsuda, Y. Tanaka, S. Maeda, F. Liu, S. Takahashi, Y. Kushida, T. Komatsu, T. Ueno, T. Terai, T. Nakazawa, M. Uchiyama, K. Morokuma, T. Nagano and K. Hanaoka, *Angew. Chem., Int. Ed.*, 2013, **52**, 13028–13032.
- 29 Q. Cai, T. Yu, W. Zhu, Y. Xu and X. Qian, *Chem. Commun.*, 2015, **51**, 14739–14741.
- 30 S. Li, J. Wang, J. Shen, B. Wu and Y. He, *ACS Macro Lett.*, 2018, **7**, 437–441.
- 31 T. Xue, X. Jia, J. Wang, J. Xiang, W. Wang, J. Du and Y. He, *Chem. – Eur. J.*, 2019, **25**, 9634–9638.
- 32 J. Rao and A. Khan, *Polym. Chem.*, 2015, **6**, 686–690.
- 33 S. A. Jenekhe and J. A. Osaheni, *Science*, 1994, **265**, 765–768.
- 34 J. Luo, Z. Xie, J. W. Y. Lam, L. Cheng, H. Chen, C. Qiu, H. S. Kwok, X. Zhan, Y. Liu, D. Zhu and B. Z. Tang, *Chem. Commun.*, 2001, 1740–1741.
- 35 Y. Hong, J. W. Y. Lam and B. Z. Tang, *Chem. Commun.*, 2009, 4332–4353.
- 36 R. Zhan, Y. Pan, P. N. Manghnani and B. Liu, *Macromol. Biosci.*, 2017, **17**, 1600433.
- 37 J. Rao, C. Hottinger and A. Khan, *J. Am. Chem. Soc.*, 2014, **136**, 5872–5875.
- 38 J. Rao and A. Khan, *J. Am. Chem. Soc.*, 2013, **135**, 14056–14059.
- 39 T. Eom, W. Yoo, S. Kim and A. Khan, *Biomaterials*, 2018, **185**, 333–347.
- 40 T. Xue, J. Shen, K. Shao, W. Wang, B. Wu and Y. He, *Chem. – Eur. J.*, 2020, **26**, 2521–2528.
- 41 D. Ross, H. D. Beall, D. Siegel, R. D. Traver and D. L. Gustafson, *Br. J. Cancer*, 1996, **74**, S1–S8.
- 42 A. Ryan, *Br. J. Pharmacol.*, 2017, **174**, 2161–2173.
- 43 M. Ravi, V. Paramesh, S. R. Kaviya, E. Anuradha and F. D. P. Solomon, *J. Cell. Physiol.*, 2015, **230**, 16–26.
- 44 E. Knight and S. Przyborski, *J. Anat.*, 2015, **227**, 746–756.